



Universiteit  
Leiden  
The Netherlands

## Electron trapping mechanism in LaAlO<sub>3</sub>/SrTiO<sub>3</sub> heterostructures

Yin, C.; Smink, A.E.M.; Leermakers, I.; Tang, L.M.K.; Lebedev, N.; Zeitler, U.; ... ; Aarts, J.

### Citation

Yin, C., Smink, A. E. M., Leermakers, I., Tang, L. M. K., Lebedev, N., Zeitler, U., ... Aarts, J. (2020). Electron trapping mechanism in LaAlO<sub>3</sub>/SrTiO<sub>3</sub> heterostructures. *Physical Review Letters*, 124(1), 017702. doi:10.1103/PhysRevLett.124.017702

Version: Publisher's Version

License: [Leiden University Non-exclusive license](#)

Downloaded from: <https://hdl.handle.net/1887/85784>

**Note:** To cite this publication please use the final published version (if applicable).

## Electron Trapping Mechanism in LaAlO<sub>3</sub>/SrTiO<sub>3</sub> Heterostructures

Chunhai Yin<sup>1</sup>, Alexander E. M. Smink,<sup>2</sup> Inge Leermakers,<sup>3</sup> Lucas M. K. Tang,<sup>3</sup> Nikita Lebedev,<sup>1</sup> Uli Zeitler,<sup>3</sup> Wilfred G. van der Wiel,<sup>2</sup> Hans Hilgenkamp,<sup>2</sup> and Jan Aarts<sup>1</sup>

<sup>1</sup>*Huygens-Kamerlingh Onnes Laboratory, Leiden University, P.O. Box 9504, 2300 RA Leiden, The Netherlands*

<sup>2</sup>*MESA+ Institute for Nanotechnology, University of Twente, P.O. Box 217, 7500 AE Enschede, The Netherlands*

<sup>3</sup>*High Field Magnet Laboratory (HFML-EMFL), Radboud University, Toernooiveld 7, 6525 ED Nijmegen, The Netherlands*



(Received 24 February 2019; revised manuscript received 13 September 2019; published 7 January 2020)

In LaAlO<sub>3</sub>/SrTiO<sub>3</sub> heterostructures, a still poorly understood phenomenon is that of electron trapping in back-gating experiments. Here, by combining magnetotransport measurements and self-consistent Schrödinger-Poisson calculations, we obtain an empirical relation between the amount of trapped electrons and the gate voltage. The amount of trapped electrons decays exponentially away from the interface. However, contrary to earlier observations, we find that the Fermi level remains well within the quantum well. The enhanced trapping of electrons induced by the gate voltage can therefore not be explained by a thermal escape mechanism. Further gate sweeping experiments strengthen that conclusion. We propose a new mechanism which involves the electromigration and clustering of oxygen vacancies in SrTiO<sub>3</sub> and argue that such electron trapping is a universal phenomenon in SrTiO<sub>3</sub>-based two-dimensional electron systems.

DOI: 10.1103/PhysRevLett.124.017702

Controlling the electronic properties of materials by applying an external voltage is at the heart of modern electronics. This is also true for oxide heterostructures, where the quasi-two-dimensional electron gas (Q2DEG) discovered at the interface between LaAlO<sub>3</sub> (LAO) and SrTiO<sub>3</sub> (STO) [1] displays a multitude of physical properties, such as superconductivity [2], signatures of magnetism [3–5] and even their coexistence [6,7]. Due to the large permittivity of the STO substrate [8], the carrier density and mobility of the Q2DEG can be modulated by a back-gate voltage ( $V_G$ ). Gate-tunable insulator to metal transitions [9], insulator to superconductor transitions [10] and Rashba spin-orbit interactions [11,12] have been reported. At the LAO/STO interface, the Q2DEG is confined in a quantum well (QW) on the STO side and the band structure is formed by the Ti  $t_{2g}$  orbitals. For LAO films grown on STO (001) substrates, the  $d_{xy}$  band lies below the  $d_{xz,yz}$  bands in energy [13–15]. Applying  $V_G$  across the STO substrate changes the carrier density in the QW. A Lifshitz transition occurs when the Fermi level is tuned across the bottom of the  $d_{xz,yz}$  bands [16]. In back-gating experiments, a commonly observed phenomenon is that the sheet resistance ( $R_s$ ) follows an irreversible route when  $V_G$  is swept first forward and then backward [10,17–20]. The explanation given by Biscaras *et al.* [18] is that the Fermi level lies intrinsically close to the top of the QW. High-mobility electrons escape and get trapped in STO when the carrier density is beyond a threshold. But the relations between the amount of trapped electrons, their spatial distribution, and the gate voltage are still unknown. We study these relations

by combining magnetotransport measurements and self-consistent Schrödinger-Poisson calculations on samples grown by sputtering and pulsed laser deposition (PLD). In both cases, the thermal escape mechanism cannot be reconciled with our results. Further gate sweeping experiments strengthen this conclusion. We propose a new mechanism which involves the electromigration and clustering of oxygen vacancies in SrTiO<sub>3</sub>. Results of the sputtered sample are discussed in the main text, those of the PLD-grown sample are in the Supplemental Material [21].

Hall bar devices were used as depicted in Fig. 1(a) (inset), of length 1000  $\mu\text{m}$  and width 150  $\mu\text{m}$ . First, a sputtered amorphous AlO<sub>x</sub> hard mask in the form of a negative Hall bar geometry (thickness  $\sim 15$  nm) was fabricated on a TiO<sub>2</sub>-terminated STO (001) substrate [26] by photolithography. Then, 15 unit cells of LAO film were deposited at 800 °C in an Ar pressure of 0.04 mbar by 90° off-axis sputtering [27]. Finally, the sample was *in situ* annealed at 600 °C in 1 mbar of oxygen for 1 h. The backgate electrode was formed by uniformly applying a thin silver paint layer (Ted Pella, Inc.) on the back of the substrate. Device fabrication details are described in the Supplemental Material [21]. The longitudinal and transverse resistances ( $R_{xx}$ ,  $R_{xy}$ ) were measured simultaneously by standard lock-in technique ( $f = 13.53$  Hz and  $i_{\text{RMS}} = 1.0$   $\mu\text{A}$ ). Magnetotransport measurements were performed under different  $V_G$  at 4.2 K in a superconducting magnet (field sweep  $\pm 15$  T). The maximum applied  $V_G$  was +200 V. The leakage current was less than 1 nA during the measurement.

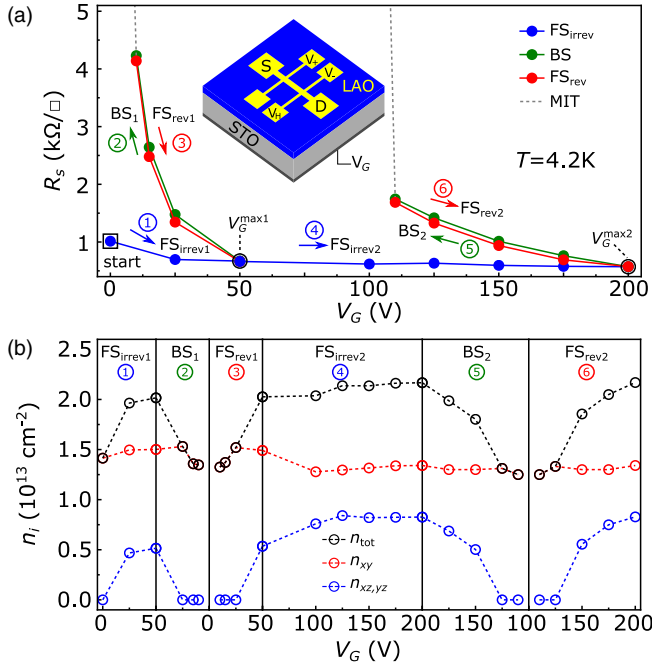


FIG. 1. (a)  $V_G$  dependence of sheet resistance ( $R_s$ ) at 4.2 K. The solid circles are  $R_s$  ( $B = 0$ ) in magnetoresistance curves. The blue, green, and red arrows indicate the irreversible forward sweep (FS<sub>irrev</sub>), backward sweep (BS), and reversible forward sweep (FS<sub>rev</sub>), respectively. The sweep order is indicated by the circled numbers. Two BSs were performed at 50 V ( $V_G^{\max 1}$ ) and 200 V ( $V_G^{\max 2}$ ). The gray dashed line indicates the metal-insulator transition (MIT). The inset shows a schematic of the Hall bar device. Source and drain are labeled as S and D. The longitudinal resistance ( $R_{xx}$ ) is measured between  $V_+$  and  $V_-$  and the transverse resistance ( $R_{xy}$ ) between  $V_H$  and  $V_-$ .  $V_G$  is applied between the back of the substrate and the drain. (b)  $V_G$  dependence of the carrier density in different regimes. The red and blue circles represent the carrier density of the  $d_{xy}$  band ( $n_{xy}$ ) and  $d_{xz,yz}$  band ( $n_{xz,yz}$ ). The black circles are the total carrier density ( $n_{tot}$ ) which is the sum of  $n_{xy}$  and  $n_{xz,yz}$ .

The device was cooled down to 4.2 K with  $V_G$  grounded. Figure 1(a) shows the  $V_G$  dependence of the sheet resistance,  $R_s$ .  $V_G$  was first increased from 0–50 V ( $V_G^{\max 1}$ ), resulting in a decrease of  $R_s$ . This sweep is called an irreversible forward sweep (FS<sub>irrev</sub>), because  $R_s$  increased above the virgin curve when  $V_G$  was swept backward. The backward sweep (BS) led to a metal-insulator transition (MIT), which is consistent with earlier reports [19]. After the onset of the MIT,  $V_G$  was further decreased to completely deplete the QW. When  $V_G$  was swept forward again,  $R_s$  followed the same route as the BS. Therefore the latter forward sweep is named a reversible forward sweep (FS<sub>rev</sub>). Another BS was performed at 200 V ( $V_G^{\max 2}$ ). It is seen that  $R_s$  increased faster in BS<sub>1</sub> than in BS<sub>2</sub>, a point to be discussed later. We also applied negative voltages. Those sweeps are always reversible, as discussed in the Supplemental Material [21].

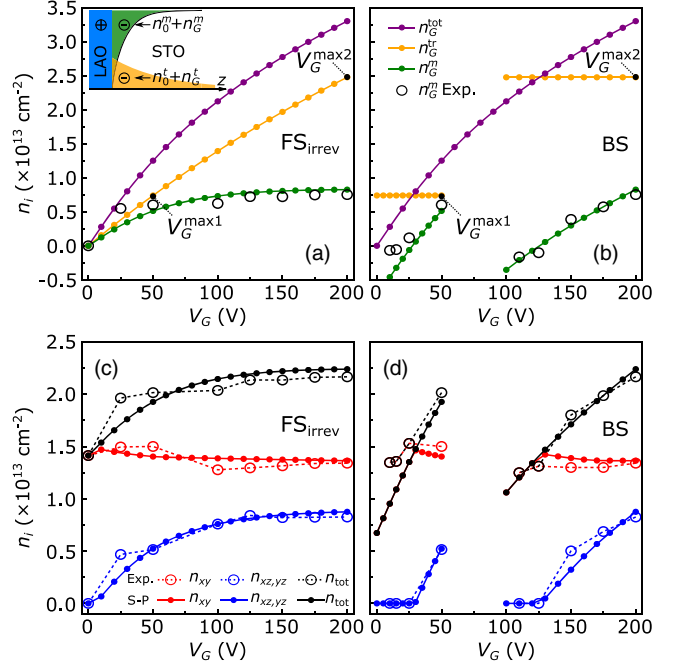


FIG. 2. (a), (b)  $V_G$  dependence of the calculated gate-induced total charge density ( $n_G^{\text{tot}}$ , purple), trapped charge density ( $n_G^{\text{tr}}$ , yellow), mobile charge density ( $n_G^{\text{m}}$ , green) and measured gate-induced mobile charge density ( $n_G^{\text{m}}$  Exp., open black circle) in (a) FS<sub>irrev</sub> and (b) BS regimes. The inset of (a) shows an illustration of the interface for Schrödinger-Poisson calculations. (c), (d)  $V_G$  dependence of S-P calculations that are calculated (solid circles) and measured (open circles)  $n_{xy}$  (red),  $n_{xz,yz}$  (blue), and  $n_{tot}$  (black) in (a) FS<sub>irrev</sub> and (b) BS regimes.

Figure 1(b) shows the  $V_G$  dependence of the carrier density of both  $d_{xy}$  ( $n_{xy}$ ) and  $d_{xz,yz}$  ( $n_{xz,yz}$ ) bands and the total carrier density ( $n_{tot}$ ). The values were extracted by fitting the magnetotransport data with a two-band model [15,21]. It can be seen that only the  $d_{xy}$  band was occupied at 0 V. In FS<sub>irrev1</sub>, electrons were added into the QW and the Lifshitz transition occurred at a carrier density ( $n_L$ ) of  $1.51 \times 10^{13} \text{ cm}^{-2}$ , which is close to earlier reported values [16]. In BS<sub>1</sub>,  $n_{tot}$  decreased to  $1.33 \times 10^{13} \text{ cm}^{-2}$  at 10 V, which is the onset of the MIT, comparable to the earlier reported carrier density ( $0.5\text{--}1.5 \times 10^{13} \text{ cm}^{-2}$ ) for the MIT [28]. In FS<sub>rev1</sub>, the carrier densities of the bands were tuned reversibly as in BS<sub>1</sub> and the system was fully recovered when 50 V was reapplied. In FS<sub>irrev2</sub>,  $n_{tot}$  saturated at  $2.17 \times 10^{13} \text{ cm}^{-2}$  beyond 125 V. In BS<sub>2</sub>, the MIT occurred at 110 V with a carrier density of  $1.25 \times 10^{13} \text{ cm}^{-2}$ , which could be due to the Hall bar contacts becoming insulating faster than the channel [29]. A noteworthy feature is that the amount of gate-induced trapped electrons is independent of the number of backward sweeps and is only related to  $V_G^{\max}$ .

First, we study the relation between the amount of trapped electrons and the gate voltage. In a backgating experiment, the total amount of electrons ( $n_G^{\text{tot}}$ ) induced by  $V_G$ , as shown by the purple curves in Figs. 2(a) and 2(b),

can be calculated using a parallel plate capacitor model [30,31]:

$$n_G^{\text{tot}}(V_G) = \int_{V_1}^{V_2} \frac{\epsilon_0}{ed_{\text{STO}}} \epsilon_r(V_G) dV_G, \quad (1)$$

where  $\epsilon_0$  is the vacuum permittivity,  $e$  is the electron charge and  $d_{\text{STO}}$  is the thickness of the STO substrate (0.5 mm). The field-dependent permittivity of the STO substrate  $\epsilon_r(V_G)$  is calculated following Ref. [32]:

$$\epsilon_r(E) = 1 + \frac{B}{[1 + (E/E_0)^2]^{1/3}}, \quad (2)$$

where the electric field  $E = V_G/d_{\text{STO}}$ ,  $B = 2.55 \times 10^4$  and  $E_0 = 8.22 \times 10^4$  V/m. In FS<sub>irrev</sub> regimes, as shown in Fig. 2(a), a part of  $n_G^{\text{tot}}$  becomes gate-induced trapped electrons ( $n_G^{\text{tr}}$ ) in STO. Subtracting  $n_G^{\text{tr}}$  from  $n_G^{\text{tot}}$  will give the amount of gate-induced mobile electrons ( $n_G^{\text{m}}$ ) which are doped into the QW. We find that the relation between  $n_G^{\text{tr}}$  and  $V_G$  can be described using the following expression:

$$n_G^{\text{tr}}(V_G) = N(1 - e^{-V_G/400}), \quad (3)$$

which yields the yellow curve, where  $N = 6.2 \times 10^{13}$  cm<sup>-2</sup>. The subtraction ( $n_G^{\text{tot}} - n_G^{\text{tr}} = n_G^{\text{m}}$ ) is given by the green curve, and gives a good description of the measured  $n_G^{\text{m}}$  (open black circle). In BS regimes, as shown in Fig. 2(b),  $n_G^{\text{tot}}$  is given by  $V_G$  according to Eq. (1). However, the value of  $n_G^{\text{tr}}$  is fixed at the  $n_G^{\text{tr}}(V_G^{\text{max}})$ . Thus,  $n_G^{\text{m}}$  is smaller than its counterpart in FS<sub>irrev</sub> regimes. In both BS regimes the calculated  $n_G^{\text{m}}$  is in good agreement with the experimental data. Moreover, due to the field-dependent permittivity,  $dn_G^{\text{tot}}/dV_G$  is decreasing as  $V_G$  increases. As a consequence, the same negative  $\Delta V_G$  removes more mobile electrons at 50 V rather than at 200 V, which could explain the fact that  $R_s$  increases faster in BS<sub>1</sub> than in BS<sub>2</sub>. It should be noted that the empirical formula of  $n_G^{\text{tr}}(V_G)$  is not universal, but instead varies among samples. We performed similar  $V_G$  sweeps on two reference samples and observed slightly different  $V_G$  dependence of  $R_s$  (see Fig. S5 in the Supplemental Material [21]). Thus,  $n_G^{\text{tr}}(V_G)$  should always be obtained from experimental results.

Next, we use the self-consistent Schrödinger-Poisson (S-P) model to study the charge distribution and band occupation [15,33–36]. S-P calculations are based on the effective mass and envelope wave function approximations. Due to the orbital orientation,  $d_{xy}$  and  $d_{xz,yz}$  orbitals are heavy and light in the  $z$  direction, respectively. We take the effective masses as  $m_{xy}^{*z} = 14 m_e$  and  $m_{xz,yz}^{*z} = 0.7 m_e$  [14,15,35], where  $m_e$  is the electron mass. We take  $z > 0$  to be STO. In the original state, there are initial mobile electrons ( $n_0^{\text{m}}$ ,  $1.41 \times 10^{13}$  cm<sup>-2</sup> in our sample) and initial trapped electrons ( $n_0^{\text{tr}}$ ) on the STO side, and an

equivalent amount of positive charges on the LAO side to keep overall charge neutrality.

The spatial distributions of the trapped electrons, both  $n_0^{\text{tr}}$  and  $n_G^{\text{tr}}(V_G)$ , are input parameters of the S-P model, which effectively influence the  $V_G$  dependent occupation of the  $d_{xy}$  and  $d_{xz,yz}$  bands. In our calculations, we obtain the best results by using the following distribution of the trapped electrons:

$$n_{3\text{D}}^{\text{tr}}(z, V_G) = \begin{cases} 0 & \text{for } z < 0 \\ \frac{n_0^{\text{tr}} + n_G^{\text{tr}}(V_G)}{\lambda} e^{-z/\lambda} & \text{for } z \geq 0 \end{cases} \quad (4)$$

where  $n_0^{\text{tr}} = 6.4 \times 10^{13}$  cm<sup>-2</sup> and  $\lambda = 50$  nm. The integration range is from 0 to 100 nm, which is divided into 2000 equal sections. The calculated evolutions of  $n_{xy}$  and  $n_{xz,yz}$  in FS<sub>irrev</sub> and BS regimes are shown in Figs. 2(c) and 2(d), closely agreeing with the experimental data.

Based on the above analysis, we could obtain the confining potential profile, the Fermi energy and the spatial distribution of mobile electrons occupying the  $d_{xy}$  and  $d_{xz,yz}$  bands. Figures 3(a)–3(c) show the results at 0, 50, and 200 V, respectively. The mobile electrons are confined within  $\sim 10$  nm at the interface, which agrees with the reported spatial distribution of the Q2DEG [37–39]. Figure 3(d) shows the confining potential in a larger range. In all cases the Fermi level is well below the top of the QW; therefore the probability of mobile electrons thermally escaping [ $k_B T(4.2 \text{ K}) \approx 0.36$  meV] from the QW should be very low. The subband dispersions of the three cases are shown in Figs. 3(e)–3(g). We note that increasing  $V_G$  decreases the spacing between the subband levels.

In order to check the thermal escape mechanism [18] in more detail, we warmed the device to room temperature to remove the trapping [17], cooled down again to 4.2 K and performed multiple backward sweeps from 10 to 50 V. As shown in Fig. 4, a growing  $R_s$  separation between FS<sub>irrev</sub> and BS is seen as  $V_G^{\text{max}}$  increases. In the thermal escape mechanism, electron trapping only occurs after  $R_s$  (or  $n_{\text{tot}}$ ) reaches its saturation. However, our experiment clearly shows that trapping occurs immediately when positive  $V_G$  is applied and the amount of trapped electrons increases as  $V_G^{\text{max}}$  increases. So we can rule out thermal escaping of mobile electrons to be the mechanism for electron trapping. We performed the same magnetotransport measurements and S-P calculations on a PLD-grown sample. Although the characteristic transport and fitting parameters of the PLD sample were very different from the sputtered one, the Fermi level was also found to stay well within the quantum well. Moreover, similar irreversible behavior has been reported in other Q2DEG systems, such as LaTiO<sub>3</sub>/STO [18], LaVO<sub>3</sub>/STO [20], (LaAlO<sub>3</sub>)<sub>0.3</sub>(Sr<sub>2</sub>AlTaO<sub>6</sub>)<sub>0.7</sub>/STO [40], and amorphous LAO/STO [41]. Therefore the electron trapping phenomenon appears intrinsic to the STO substrate. We also checked whether the structural

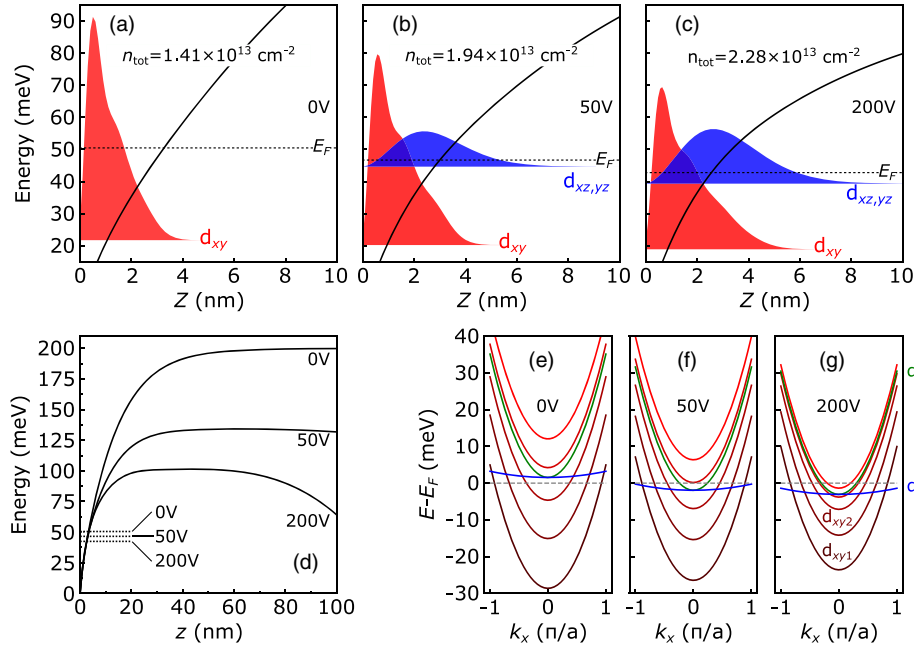


FIG. 3. (a)–(c) S-P calculations confining potential profile (solid line), Fermi energy (dotted line), and spatial distribution of mobile electrons occupying  $d_{xy}$  (red) and  $d_{xz,yz}$  (blue) bands at (a) 0, (b) 50, and (c) 200 V. (d) Confining potential and Fermi energy in a larger range. (e), (f) S-P calculated subband dispersions in parabolic approximation at (e) 0, (f) 50, and (g) 200 V.

phase transition of the STO substrate at 105 K plays a role in the trapping [42–44]. Gating experiments at 4, 80, and 120 K all showed hysteresis, as shown in the Supplemental Material [21]. We conclude that tetragonal domain formation is not important for what we observe.

We propose a two-step trapping mechanism involving redistribution of oxygen vacancies ( $V_O$ 's) in STO under influence of an electric field. The first step is the electromigration of  $V_O$ 's. Among all types of defects in STO,  $V_O$  has the lowest activation enthalpy for migration [45] as reported in previous works [46–48]. The second step is the clustering of  $V_O$ 's which could form in-gap trapping states [49,50], of which the energy was recently determined to be

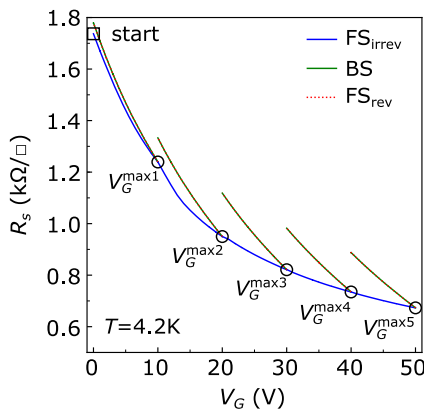


FIG. 4.  $V_G$  dependence of  $R_s$  at 4.2 K. The sweep order is similar to that in Fig. 1(a). Backward sweeps were performed from 10 to 50 V. Note that BS and  $FS_{rev}$  overlap perfectly.

$\sim 0.31$  and  $\sim 1.11$  eV below the conduction band [51]. Figure 5 shows the dynamic resistance change during and after  $V_G$  sweeps in the  $FS_{irrev}$  and BS regimes. The electron trapping mechanism can then be explained as follows. In  $FS_{irrev}$  regimes as shown in Fig. 5(a), the effect of

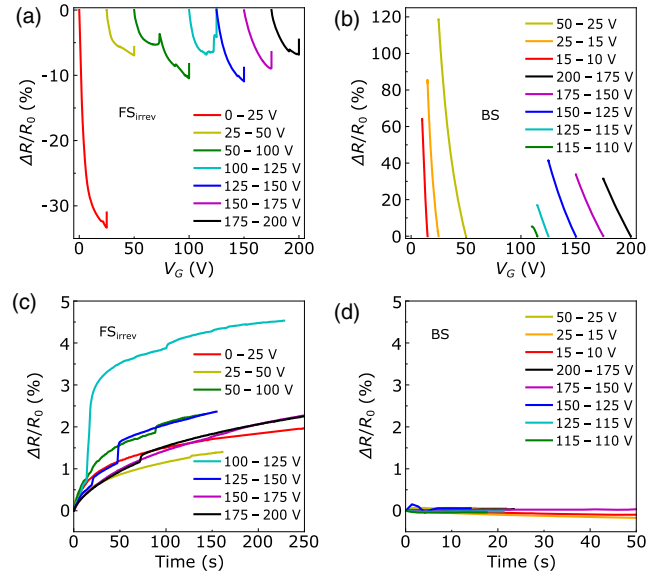


FIG. 5. (a), (b) Dynamic change of  $R_s$  during  $V_G$  sweeps in (a)  $FS_{irrev}$  and (b) BS regimes.  $V_G$  was swept at a rate of 0.1 V/s.  $R_s$  measurements kept on going for several minutes after the stabilization of  $V_G$ . (c), (d) Dynamic change of  $R_s$  after  $V_G$  sweeps in (c)  $FS_{irrev}$  and (d) BS regimes.



increasing  $V_G$  is twofold. One is to add electrons into the QW. The other is to push positively charged  $V_O$ 's migrating toward the interface. The clustering of the accumulated  $V_O$ 's then forms in-gap trapping states. Several sudden resistance jumps can be clearly seen during  $V_G$  sweeps, which might be due to the formation of big  $V_O$  clusters. Moreover, after stabilizing the gate voltage as shown in Fig. 5(c), the electromigration and clustering of  $V_O$ 's do not stop immediately. Newly formed in-gap states still trap conduction electrons, resulting in an immediate increase of  $R_s$  when  $V_G$  stabilizes. In BS and FS<sub>rev</sub> regimes as shown in Figs. 5(b) and 5(d), sweeping  $V_G$  only changes the carrier density in the QW without modifying the defect landscape near the interface. Therefore the system can be tuned in a reversible manner. A schematic illustration of our proposed electric field-driven trapping mechanism is shown in the Supplemental Material [21].

Summarizing, we studied electron trapping in LAO/STO heterostructures under backgate voltages. Combined magnetotransport measurements and self-consistent Schrödinger-Poisson calculations yield a relation between the amount of trapped electrons and the gate voltage as well as the spatial distribution of the trapped electrons. We propose a new trapping mechanism which involves the electromigration and clustering of oxygen vacancies in STO, since our analysis shows that the thermal escape mechanism is not valid. This is relevant for theoretical works [35,52,53], where the assumption was that all the gate-induced electrons land in the QW. We obtained qualitatively similar results from the samples grown by sputtering and PLD, and conclude that electron trapping is a universal phenomenon in SrTiO<sub>3</sub>-based two-dimensional electron systems.

We thank Nicandro Bovenzi, Andrea Caviglia, Stefano Gariglio, Haijiao Harsan Ma, Yulin Gan, Felix Gunkel, Kevin Steffen, Prateek Kumar, and Aymen Ben Hamida for discussions and Anatolie Mitiglu and Lisa Rossi for technical assistance. This work is supported by the Netherlands Organisation for Scientific Research (NWO) through the DESCO program. We acknowledge the support of HFML-RU/NWO, member of the European Magnetic Field Laboratory (EMFL). C. Y. is supported by China Scholarship Council (CSC) with Grant No. 201508110214.

---

[1] A. Ohtomo and H. Y. Hwang, *Nature (London)* **427**, 423 (2004).  
 [2] N. Reyren, S. Thiel, A. D. Caviglia, L. F. Kourkoutis, G. Hammerl, C. Richter, C. W. Schneider, T. Kopp, A.-S. Ruetschi, D. Jaccard, M. Gabay, D. A. Muller, J.-M. Triscone, and J. Mannhart, *Science* **317**, 1196 (2007).  
 [3] A. Brinkman, M. Huijben, M. V. Zalk, J. Huijben, U. Zeitler, J. C. Maan, W. G. V. D. Wiel, G. Rijnders, D. H. A. Blank, and H. Hilgenkamp, *Nat. Mater.* **6**, 493 (2007).

[4] Ariando, X. Wang, G. Baskaran, Z. Q. Liu, J. Huijben, J. B. Yi, A. Annadi, A. R. Barman, A. Rusydi, S. Dhar, Y. P. Feng, J. Ding, H. Hilgenkamp, and T. Venkatesan, *Nat. Commun.* **2**, 188 (2011).  
 [5] J.-S. Lee, Y. W. Xie, H. K. Sato, C. Bell, Y. Hikita, H. Y. Hwang, and C.-C. Kao, *Nat. Mater.* **12**, 703 (2013).  
 [6] L. Li, C. Richter, J. Mannhart, and R. C. Ashoori, *Nat. Phys.* **7**, 762 (2011).  
 [7] J. A. Bert, B. Kalisky, C. Bell, M. Kim, Y. Hikita, H. Y. Hwang, and K. A. Moler, *Nat. Phys.* **7**, 767 (2011).  
 [8] R. C. Neville, B. Hoeneisen, and C. A. Mead, *J. Appl. Phys.* **43**, 2124 (1972).  
 [9] S. Thiel, G. Hammerl, A. Schmehl, C. W. Schneider, and J. Mannhart, *Science* **313**, 1942 (2006).  
 [10] A. D. Caviglia, S. Gariglio, N. Reyren, D. Jaccard, T. Schneider, M. Gabay, S. Thiel, G. Hammerl, J. Mannhart, and J.-M. Triscone, *Nature (London)* **456**, 624 (2008).  
 [11] M. Ben Shalom, M. Sachs, D. Rakhmievitch, A. Palevski, and Y. Dagan, *Phys. Rev. Lett.* **104**, 126802 (2010).  
 [12] A. D. Caviglia, M. Gabay, S. Gariglio, N. Reyren, C. Cancellieri, and J.-M. Triscone, *Phys. Rev. Lett.* **104**, 126803 (2010).  
 [13] M. Salluzzo, J. C. Cezar, N. B. Brookes, V. Bisogni, G. M. De Luca, C. Richter, S. Thiel, J. Mannhart, M. Huijben, A. Brinkman, G. Rijnders, and G. Ghiringhelli, *Phys. Rev. Lett.* **102**, 166804 (2009).  
 [14] A. F. Santander-Syro, O. Copie, T. Kondo, F. Fortuna, S. Pailhès, R. Weht, X. G. Qiu, F. Bertran, A. Nicolaou, A. Taleb-Ibrahimi, P. Le Fèvre, G. Herranz, M. Bibes, N. Reyren, Y. Apertet, P. Lecoeus, A. Barthélémy, and M. J. Rozenberg, *Nature (London)* **469**, 189 (2011).  
 [15] A. E. M. Smink, J. C. de Boer, M. P. Stehno, A. Brinkman, W. G. van der Wiel, and H. Hilgenkamp, *Phys. Rev. Lett.* **118**, 106401 (2017).  
 [16] A. Joshua, S. Pecker, J. Ruhman, E. Altman, and S. Ilani, *Nat. Commun.* **3**, 1129 (2012).  
 [17] C. Bell, S. Harashima, Y. Kozuka, M. Kim, B. G. Kim, Y. Hikita, and H. Y. Hwang, *Phys. Rev. Lett.* **103**, 226802 (2009).  
 [18] J. Biscaras, S. Hurand, C. Feuillet-Palma, A. Rastogi, R. C. Budhani, N. Reyren, E. Lesne, J. Lesueur, and N. Bergeal, *Sci. Rep.* **4**, 6788 (2015).  
 [19] W. Liu, S. Gariglio, A. Fête, D. Li, M. Boselli, D. Stornaiuolo, and J.-M. Triscone, *APL Mater.* **3**, 062805 (2015).  
 [20] H. Liang, L. Cheng, L. Wei, Z. Luo, G. Yu, C. Zeng, and Z. Zhang, *Phys. Rev. B* **92**, 075309 (2015).  
 [21] See Supplemental Material at <http://link.aps.org/supplemental/10.1103/PhysRevLett.124.017702> for device fabrication, measurements, two-band model fitting, S-P calculations on sputtered and PLD-grown samples, and a schematic illustration of the trapping mechanism, which includes Refs. [22–25].  
 [22] N. Banerjee, M. Huijben, G. Koster, and G. Rijnders, *Appl. Phys. Lett.* **100**, 041601 (2012).  
 [23] P. D. Eerkes, W. G. van der Wiel, and H. Hilgenkamp, *Appl. Phys. Lett.* **103**, 201603 (2013).  
 [24] D. Rakhmievitch, I. Neder, M. B. Shalom, A. Tsukernik, M. Karpovskii, Y. Dagan, and A. Palevski, *Phys. Rev. B* **87**, 125409 (2013).

- [25] C. Richter, H. Boschker, W. Dietsche, E. Fillis-Tsirakis, R. Jany, F. Loder, L. F. Kourkoutis, D. A. Muller, J. R. Kirtley, C. W. Schneider, and J. Mannhart, *Nature (London)* **502**, 528 (2013).
- [26] G. Koster, B. L. Kropman, G. J. H. M. Rijnders, D. H. A. Blank, and H. Rogalla, *Appl. Phys. Lett.* **73**, 2920 (1998).
- [27] C. Yin, D. Krishnan, N. Gauquelin, J. Verbeeck, and J. Aarts, *Phys. Rev. Mater.* **3**, 034002 (2019).
- [28] Y. C. Liao, T. Kopp, C. Richter, A. Rosch, and J. Mannhart, *Phys. Rev. B* **83**, 075402 (2011).
- [29] A. E. M. Smink, M. P. Stehno, J. C. de Boer, A. Brinkman, W. G. van der Wiel, and H. Hilgenkamp, *Phys. Rev. B* **97**, 245113 (2018).
- [30] K. S. Novoselov, A. K. Geim, S. V. Morozov, D. Jiang, Y. Zhang, S. V. Dubonos, I. V. Grigorieva, and A. A. Firsov, *Science* **306**, 666 (2004).
- [31] T. Ihn, *Semiconductor Nanostructures: Quantum States and Electronic Transport* (Oxford University Press, Oxford, 2015).
- [32] S. Gariglio, A. Fête, and J.-M. Triscone, *J. Phys. Condens. Matter* **27**, 283201 (2015).
- [33] F. Stern, *Phys. Rev. B* **5**, 4891 (1972).
- [34] J. Biscaras, N. Bergeal, S. Hurand, C. Grossetête, A. Rastogi, R. C. Budhani, D. Le Boeuf, C. Proust, and J. Lesueur, *Phys. Rev. Lett.* **108**, 247004 (2012).
- [35] N. Scopigno, D. Bucheli, S. Caprara, J. Biscaras, N. Bergeal, J. Lesueur, and M. Grilli, *Phys. Rev. Lett.* **116**, 026804 (2016).
- [36] D. Li, S. Lemal, S. Gariglio, Z. Wu, A. Fête, M. Boselli, P. Ghosez, and J.-M. Triscone, *Adv. Sci.* **5**, 1800242 (2018).
- [37] M. Basletic, J.-L. Maurice, C. Carrétéro, G. Herranz, O. Copie, M. Bibes, E. Jacquet, K. Bouzehouane, S. Fusil, and A. Barthélémy, *Nat. Mater.* **7**, 621 (2008).
- [38] M. Sing, G. Berner, K. Goß, A. Müller, A. Ruff, A. Wetscherek, S. Thiel, J. Mannhart, S. A. Pauli, C. W. Schneider, P. R. Willmott, M. Gorgoi, F. Schäfers, and R. Claessen, *Phys. Rev. Lett.* **102**, 176805 (2009).
- [39] N. Reyren, S. Gariglio, A. D. Caviglia, D. Jaccard, T. Schneider, and J.-M. Triscone, *Appl. Phys. Lett.* **94**, 112506 (2009).
- [40] V. V. Bal, Z. Huang, K. Han, Ariando, T. Venkatesan, and V. Chandrasekhar, *Appl. Phys. Lett.* **111**, 081604 (2017).
- [41] A. V. Bjørli, M. V. Soosten, R. Erlandsen, R. T. Dahm, Y. Zhang, Y. Gan, Y. Chen, N. Pryds, and T. S. Jespersen, *Appl. Phys. Lett.* **112**, 171606 (2018).
- [42] B. Kalisky, E. M. Spanton, H. Noad, J. R. Kirtley, K. C. Nowack, C. Bell, H. K. Sato, M. Hosoda, Y. Xie, Y. Hikita, C. Woltmann, G. Pfanzelt, R. Jany, C. Richter, H. Y. Hwang, J. Mannhart, and K. A. Moler, *Nat. Mater.* **12**, 1091 (2013).
- [43] H. J. Harsan Ma, S. Scharinger, S. W. Zeng, D. Kohlberger, M. Lange, A. Sthr, X. R. Wang, T. Venkatesan, R. Kleiner, J. F. Scott, J. M. D. Coey, D. Koelle, and Ariando, *Phys. Rev. Lett.* **116**, 257601 (2016).
- [44] Y. Frenkel, N. Haham, Y. Shperber, C. Bell, Y. Xie, Z. Chen, Y. Hikita, H. Y. Hwang, E. K. H. Salje, and B. Kalisky, *Nat. Mater.* **16**, 1203 (2017).
- [45] V. Metlenko, A. H. H. Ramadan, F. Gunkel, H. Du, H. Schraknepper, S. Hoffmann-Eifert, R. Dittmann, R. Waser, and R. A. D. Souza, *Nanoscale* **6**, 12864 (2014).
- [46] J. Hanzig, M. Zschornak, F. Hanzig, E. Mehner, H. Stöcker, B. Abendroth, C. Röder, A. Talkenberger, G. Schreiber, D. Rafaja, S. Gemming, and D. C. Meyer, *Phys. Rev. B* **88**, 024104 (2013).
- [47] Y. Lei, Y. Li, Y. Z. Chen, Y. W. Xie, Y. S. Chen, S. H. Wang, J. Wang, B. G. Shen, N. Pryds, H. Y. Hwang, and J. R. Sun, *Nat. Commun.* **5**, 5554 (2014).
- [48] Y. Li, S. J. Peng, T. T. Mao, D. J. Wang, K. M. Wu, J. R. Sun, and J. Zhang, *AIP Adv.* **7**, 055821 (2017).
- [49] N. Shanthi and D. D. Sarma, *Phys. Rev. B* **57**, 2153 (1998).
- [50] D. D. Cuong, B. Lee, K. M. Choi, H.-S. Ahn, S. Han, and J. Lee, *Phys. Rev. Lett.* **98**, 115503 (2007).
- [51] C. Baeumer, C. Funck, A. Locatelli, T. O. Menteş, F. Genuzio, T. Heisig, F. Hensling, N. Raab, C. M. Schneider, S. Menzel, R. Waser, and R. Dittmann, *Nano Lett.* **19**, 54 (2019).
- [52] S. Caprara, F. Peronaci, and M. Grilli, *Phys. Rev. Lett.* **109**, 196401 (2012).
- [53] D. Bucheli, M. Grilli, F. Peronaci, G. Seibold, and S. Caprara, *Phys. Rev. B* **89**, 195448 (2014).